Formation of Ge Nanoripples on Vicinal Si (1110): From Stranski-Krastanow Seeds to a Perfectly Faceted Wetting Layer

G. Chen,[1] B. Sanduijav,[1] D. Matei,[1] G. Springholz,[1,*] D. Scopece,[2] M. J. Beck,[3] F. Montalenti,[2] and L. Miglio[2]

[1]*Institut für Halbleiter- und Festkörperphysik, Johannes Kepler University, A-4040 Linz, Austria*

[2]*L-NESS and Department of Materials Science, Università di Milano-Bicocca, Milano, Italy*

[3]*Department of Chemical and Materials Engineering, University of Kentucky, Lexington, Kentucky 40506, USA*

(Received 4 September 2011; revised manuscript received 21 November 2011; published 31 January 2012)

Ge growth on high-indexed Si (1110) is shown to result in the spontaneous formation of a perfectly {105} faceted one-dimensional nanoripple structure. This evolution differs from the usual Stranski-Krastanow growth mode because from initial ripple seeds a faceted Ge layer is formed that extends down to the heterointerface. *Ab initio* calculations reveal that ripple formation is mainly driven by lowering of surface energy rather than by elastic strain relief and the onset is governed by the edge energy of the ripple facets. Wavelike ripple replication is identified as an effective kinetic pathway for the transformation process.

DOI: 10.1103/PhysRevLett.108.055503 PACS numbers: 81.07.−b, 68.37.Ef, 68.55.A−, 81.15.Hi

Faceting plays a crucial role for Stranski-Krastanow (SK) growth of self-assembled quantum dots, where well separated three-dimensional (3D) nanoislands form on top of a flat 2D wetting layer [1–7]. The shape of these islands sensitively depends on the interplay between volumetric strain relaxation and surface energy costs [2,8,9]. This leads to characteristic island shapes defined by few high-indexed, but relatively low-energy side facets [3–9]. For the prototypical Ge/Si (001) system, therefore, a well-defined transition from pyramids [10] to domes [3–6], barns [5], or cupola islands [11] occurs as a function of coverage and growth conditions. Evidently, the energy balance is also affected by the substrate orientation. Therefore, the shape of SK islands becomes increasingly asymmetric when the substrate is tilted away from the high-symmetry (001) direction [12–17]. In the limiting case of the 8.05° miscut Si (1110) surface, as a result, 1D nanoripples instead of 3D islands [15–18] are formed. These ripples exhibit interesting physical properties because the edge contributions from the intersections between side facets scale differently with volume compared to 3D islands, where the edge energies are eventually overtaken by volumetric and surface terms [8,19]. Thus, in 1D structures edge contributions are expected to play an important role. One-dimensional structures also exhibit interesting optical and quantum transport behavior [20] and have a great potential for practical device applications [21].

In this Letter, the growth behavior of Ge on Si (1110) is studied both experimentally and theoretically combining *in situ* scanning tunneling microscopy (STM), electron diffraction, and total energy calculations. It is demonstrated that the surface evolution completely differs from the usual SK growth mode in that at the critical coverage, instead of islands a perfectly {105} faceted wetting layer is formed. Moreover, the resulting quasiperiodic ripple structure leaves no part of the original (1110) surface exposed and extends down to the Si/Ge interface. Thus, the 2D wetting layer is consumed in the transformation process. Modeling of this unique behavior by total energy calculations combining elastic continuum and density functional theory, we show that the usually neglected edge energy is a decisive parameter that determines the onset of the faceting process. To elucidate the abrupt nature of the faceting transition, a mechanism for cooperative ''wavelike'' ripple generation is devised that explains not only the consumption of the wetting layer but also the remarkable uniformity of the ripple structure.

The growth experiments were performed in a multichamber molecular beam epitaxy system, allowing sequential deposition and imaging of the epitaxial surface without exposure to ambient conditions [16]. After oxide desorption and 40 nm Si buffer growth, Ge was deposited on Si (1110) substrates at 550 °C in 0.5 monolayer (ML) increments up to a total thickness of 7 ML. Here, one ML (~ 1.4 Å) is defined as number of atoms contained in one atomic layer of Si (001) and the Ge growth rate was set to 1.1 Å/min. At the given growth temperature, little Si/Ge intermixing occurs as shown in Refs. [22,23]. After each growth step, the samples were quenched to room temperature and imaged *in situ* by STM with negative sample bias of 2–4 V. For control experiments and *in situ* reflection high energy electron diffraction (RHEED) studies, several ML were deposited in one single step, giving essentially the same results as for the stepwise grown samples.

After buffer growth, the clean Si (1110) surface displays a regular structure, consisting of narrow ~1.9 nm wide (001) terraces separated by straight double monolayer D_B steps parallel to the $[\bar{1}10]$ surface direction. The terraces exhibit the typical (2×1) surface reconstruction with dimer rows perpendicular to the step edges and the rebonding of the D_B steps reduces the number of dangling bonds [24,25]. Upon Ge deposition, the long terraces break up

into short segments of varying length and with further deposition, shorter and shorter terrace segments are formed [15]. Moreover, the missing dimer rows of adjacent terraces start to line up along the [55$\bar{1}$] surface direction. This leads to the formation of 1–2 ML deep trenches along the miscut direction. As revealed by the STM image depicted in Fig. 1(a) for 3.6 ML Ge coverage these evolve into elongated mounds that resemble the shallow Stranski-Krastanow seeds observed for subcritical Ge growth on Si (001) [26]. The elongated mounds have typical widths of 5–10 nm and lengths of 15–30 nm [cf. Fig. 1(b)] and their sidewalls are formed by small areas with local {105} surface orientation. This leads to the appearance of weak {105} facet spots in the surface orientation density map (SOM) of the STM image which is shown as inset in Fig. 1(a).

The isolated ripple seeds persist up to 4 ML coverage without much change in amplitude or size. At a critical coverage of 4.2 ML, however, a dramatic and sudden surface transition occurs by which the whole epilayer surface is rapidly transformed to a perfectly {105} faceted, quasiperiodic 1D ripple structure. This is demonstrated by the STM images displayed in Figs. 1(c) and 1(d) recorded at 4.5 ML Ge coverage. As revealed by the high-resolution STM image of Fig. 1(c), the sidewalls of the ripples exhibit

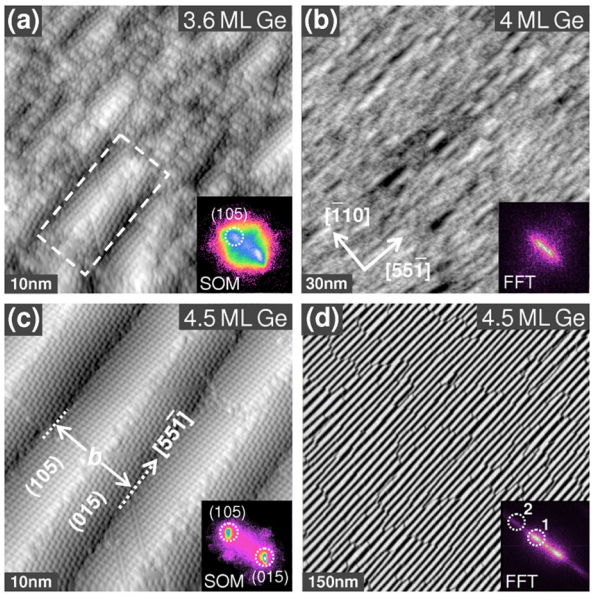

FIG. 1 (color online). STM images of Ge on Si (1110) deposited at 550 °C recorded at coverages of (a) 3.7 ML, (b) 4.0 ML, and 4.5 ML for (c) and (d). Note the different scale of the images. The insets in (a) and (c) depict the surface orientation maps (SOM) calculated from larger STM images, revealing complete {105} facetation of the Ge surface at thicknesses exceeding 4.2 ML. Only isolated mounds and prerippples are seen for lower coverages. The insets in (b) and (d) show the 2D FFT power spectra of the STM images. For the perfectly faceted Ge surface at 4.5 ML, FFT satellite peaks (indicated by circles) up to the second order are observed.

the characteristic zigzag structure of the rebonded-step {105} surface reconstruction [27,28]. Moreover, the STM surface orientation map depicted as the inset exhibits now only two sharp maxima at the {105} positions. This underlines that the nanoripples seamlessly cover the whole epilayer surface and nowhere is the original (1110) surface exposed. As demonstrated by the large scale STM image presented in Fig. 1(d), the ripples are perfectly aligned along the [55$\bar{1}$] miscut direction and they are remarkably uniform in size. Their height is 1.2 nm and their average width 17 nm as derived from statistical analysis, and their length well exceeds 300 nm.

The abruptness of the ripple transition is demonstrated by *in situ* RHEED experiments presented in Figs. 2(a)–2(d). Upon ripple formation, the diffraction pattern drastically changes due to scattering from the ripple facets. Accordingly, the RHEED pattern after ripple formation [Fig. 2(d)] shows strong facet diffraction spots (FS) and the specular spot (SS) essentially disappears. For quantitative analysis, in Fig. 2(a) the intensity evolution of the

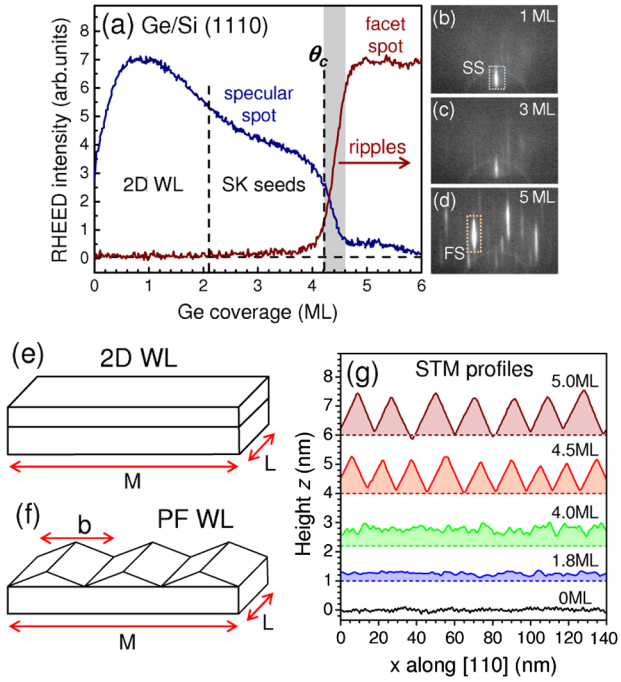

FIG. 2 (color online). (a) RHEED intensity of the specular spot (SS, blue line) and a facet diffraction spot (FS, black line) plotted as a function of Ge coverage on Si (1110), indicating an abrupt morphological transition at a critical coverage of 4.2 ML. RHEED patterns recorded at different coverages are shown in (b) to (d). The schematic illustration of the flat 2D wetting layer (WL) and the perfectly faceted (PF) ripple surface are shown in (e) and (f), respectively. Panel (g) shows the evolution of the surface profile along [−110] as a function of Ge coverage. The shaded regions below the profiles represent the respective total Ge amount deposited in each case and the horizontal dashed lines the location of the Ge/Si heterointerface. For clarity, the profiles are offset in the vertical direction.

specular spot and the facet spot indicated in Fig. 2(d) is plotted as a function of Ge coverage, evidencing a sharp onset of ripple formation at a critical coverage of 4.2 ML and a completion of the transformation process within a fraction of a monolayer.

The ripple transition exhibits several remarkable features, distinguishing it from the common SK evolution observed, e.g., for Ge on Si (001) [3–5,9]. First, the ripples completely cover the whole epilayer surface, i.e., initial ripple seeds do not evolve into isolated SK islands, but the layer as a whole is transformed to a nonplanar faceted wetting layer (WL) as is shown schematically in Figs. 2(e) and 2(f). Notably, nowhere does the original (1110) surface remains exposed. Second, the ripples display a remarkable uniformity and quasiperiodic lateral ordering. This is proven by the appearance of even second order satellite peaks in the 2D Fourier transform (FFT) power spectrum of the STM image shown in Fig. 1(d). The ordered configuration with a high degree of correlation is in contrast to uncorrelated island nucleation seen for the usual SK growth mode. Third, whereas SK islands grow on top of a 2D WL, the 1D ripple transition consumes most of the layer beneath the ripple seeds; i.e., the ripples extend all the way down to the Si/Ge interface. This is revealed by STM analysis of the ripple volume per unit area V_R/A using

$$\frac{V_R}{A} = \frac{1}{2} b \frac{hl}{bl} = \frac{1}{2} h = \frac{1}{4} b \tan\varphi, \tag{1}$$

where the ripple sidewall angle $\varphi = 7.97°$ is fixed by the {105} ripple geometry and the ripple period of $b = 16.8$ nm is precisely derived from the FFT satellite spacings. This yields that at 4.5 ML coverage, 4.1 ML, i.e., nearly all material is contained in the ripples. Since at the growth temperature of 550 °C Si/Ge intermixing is rather small [22,23], this leaves less than half a ML of Ge at the heterointerface below the ripples. This is contrary to SK Ge island growth on Si (001), where for the same growth conditions we find that the only the material exceeding the critical thickness is contained within the islands. Finally, the perfect ripple array also displays a remarkable stability upon postgrowth annealing, showing no signs of coarsening even for extended annealing cycles at 550 °C. This indicates that the {105} faceted configuration represents a significant local minimum in the total energy of the system.

To shed light on the nature of the ripple transition, we have studied the energetics and kinetic pathways for ripple formation. The latter is of particular interest because it is difficult to conceive how the usual incoherent and uncorrelated SK island nucleation could lead to such a perfectly faceted ripple surface. At the critical coverage θ_c, obviously at least one infinitely long SK ripple seed must be stable on the surface, meaning that beyond a certain WL thickness N (in MLs) it is energetically more favorable to accumulate material in a ripple with base b and length L rather than to distribute it evenly over a $N + 1$ ML 2D WL surface. The corresponding total energy difference between these two configurations $\Delta E_{\text{tot}} = \Delta E_{\text{vol}} + \Delta E_{\text{surf}} + \Delta E_{\text{edge}}$ is calculated taking volumetric, surface as well as edge energy costs into account.

The volumetric energy change per unit length can be written as

$$\frac{\Delta E_{\text{vol}}}{L} = \frac{b^2 \tan\varphi}{4}\left(\rho_R - \rho_{\text{WL}} + \frac{\gamma_{\text{WL}}^{1110}(N) - \gamma_{\text{WL}}^{1110}(N+1)}{h_{\text{ML}}}\right) \tag{2}$$

The first term contains the differences in elastic energy densities $\Delta\rho = \rho_R - \rho_{\text{WL}}$ between the ripple and the biaxially strained WL. For pure Ge ripples and WL, the energy density $\rho_{\text{WL}} = 1.624$ meV/Å^3 was computed by the finite element method [9], revealing only a tiny relaxation $\Delta\rho/\rho_{\text{WL}} \approx -10\%$ by the shallow ripple geometry. The second term in (2) is determined by the WL surface energy difference $\gamma_{\text{WL}}^{1110}(N) - \gamma_{\text{WL}}^{1110}(N+1)$ when N is incremented to $N + 1$, divided by the height of the monolayer $h_{\text{ML}} \sim 1.4$ Å. This difference results from the strong decrease of the $\gamma_{\text{WL}}^{1110}(N)$ surface energy in the first few MLs due to decaying electronic effects from the Si interface, similar as for the Ge on Si (001) case [29]. The surface energy term ΔE_{surf} is determined by the surface energy difference when one ML is added on top of the WL instead of covering the Nth ML surface by the basal area of a ripple. It is given by

$$\Delta E_{\text{surf}}/L = b(\sec\varphi\,\gamma_R^{105} - \gamma_{\text{WL}}^{1110}(N)) \tag{3}$$

where γ_R^{105} is the averaged surface energy of the {105} ripple facets. Finally, the edge energy term ΔE_{edge} is given by

$$\Delta E_{\text{edge}}/L = 3\Gamma, \tag{4}$$

where 3Γ is the triple edge energy at the top and two basal ripple facet intersections.

Both $\gamma_{\text{WL}}^{1110}$ versus N and the average facet surface energy γ_R^{105} were computed by *ab initio* density functional theory using a double stepped D_b model for the (1110) surface [21,30] and the rebonded-step RS structure for the (105) surface [29]. The anisotropic strain across the ripple facets due to elastic strain relaxation was also included. The derived results for $N = 1$ to 5 ML entering in Eq. (2) and (3) are listed in Table I and the details about the complex *ab initio* calculations are reported separately [30]. The important outcome is that $\gamma_{\text{WL}}^{1110} > \gamma_R^{105}$, i.e., $\Delta E_{\text{surf}} < 0$ for any N value, meaning that the {105} facets are always lower in energy than the (1110) WL surface. Considering the low $\Delta\rho$ value for the shallow ripple geometry, from Table I one sees that the volumetric energy term ΔE_{vol} term [Eq. (2)] is dominated by the lowering of the WL surface

TABLE I. Free surface energy of the (1110) 2D Ge wetting layer γ_{WL}^{1110} and average (105) ripple facet surface energy γ_R^{105} for the geometries of Figs. 2(e) and 2(f) derived from density functional theory calculations as a function of Ge coverage θ_{Ge} as described in detail in Ref. [30]. The averaged surface energy of the ripples takes into account the influence of the Si substrate for the lower part of the facets as well as the actual surface strain state across the ripples due to elastic relaxation.

θ_{Ge} [001 ML]	γ_{WL}^{1110} [meV/Å^2]	γ_R^{105} [meV/Å^2]
1	75.2	72.5
2	68.4	65.9
3	65.3	62.9
4	63.8	61.3
5	63.1	60.3

energy with increasing N. Thus, strain relaxation plays a minor role in this system.

Since the edge energy is difficult to determine by *ab initio* calculations, in Fig. 3, the results for $\Delta E_{tot}/L - 3\Gamma$ as a function of ripple base b for different WL thicknesses N are presented. For all reported N, an energy minimum is found, meaning that a preferred ripple width exists. As already discussed in Ref. [9], this feature is characteristic for shallow islands with poor strain relaxation and strong surface stabilization with respect to the WL. For $N = 2.6$ ML, theory predicts an optimal ripple width $b \sim 10$ nm (vertical band in Fig. 3). This is in agreement with the experimental observations of Fig. 1(c) at $\theta_{Ge} = 3.6$ ML, from which it is estimated that a volume corresponding to 1 ML Ge is already incorporated in the ripple seeds, accounting for the difference in N and θ_{Ge}. Since we observe indefinite ripple elongation close to this coverage in annealing experiments [31], we take this value as the critical condition for infinite ripple elongation

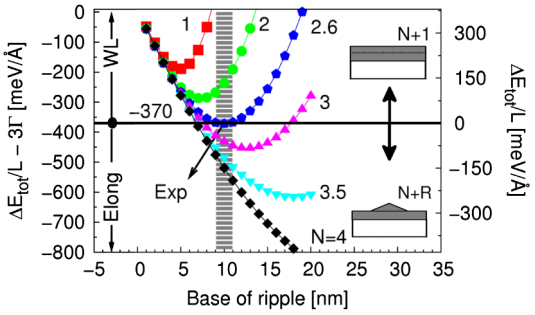

FIG. 3 (color online). Energy difference $\Delta E_{tot}/L - 3\Gamma (= \Delta E_{vol}/L + \Delta E_{surf}/L)$ calculated using Eqs. (2) and (3) between an infinitely long {105} faceted ripple on a N ML thick WL and the $N + 1$ ML thick 2D WL with the same volume plotted as a function of ripple base b at different coverages N (left axis). The horizontal line represents the value of $-E_{edge}/L = -3\Gamma = -370$ meV obtained by comparison with experiments (vertical shaded bar). The right-hand axis shows the total energy $\Delta E_{tot}/L$ of the system using this value.

corresponding to $\Delta E_{tot} = 0$ for the system. This means that at this coverage prerippples would start to grow, but the thermodynamic driving force is still too small to make the first elongation attempts successful [cf. Fig. 1(a)]. Setting $\Delta E_{tot} = 0$ for $N = 2.6$ in Fig. 3 therefore, provides a good estimate for the edge energy of the ripples of $3\Gamma = 370$ meV/Å as indicated by the horizontal line. This is notably larger than previously derived theoretical values [19] using, however, classical approaches and idealized geometries. On the other hand, from the high-resolution STM image of Fig. 1(c) it is evident that contributions to the edge energy 3Γ at the intersections of the ripple facets actually come from a 2D surface region as wide as 3 nm, where the local {105} reconstruction geometry is strongly changed. The $3\Gamma = 370$ meV/Å value, therefore, contains contributions from a rather wide area with an extra surface energy of around 10 meV/Å^2 with respect to {105}, which is in line with typical differences between alternative surface reconstructions [29]. Setting 3Γ to 370 meV/Å, we straightforwardly obtain the variation of E_{tot}/L as represented by the right-hand scale of Fig. 3. While the results are shown only for the pure Ge case, allowing for small amounts of Si intermixing into the ripples does not alter our predictions because of the minor role played by strain relaxation.

Figure 3 allows us to extract further information on the system behavior. According to it, once the critical thickness is reached, ripples would simply grow larger with increasing deposition as the minimum energy shifts to larger basewidths, thereby mimicking a typical SK behavior. This is, however, inconsistent with the experimental results. To this end, an alternative mechanism is proposed to account for the abrupt faceting transition in an efficient and correlated way. As shown schematically in Fig. 4(a), we propose a wavelike lateral ripple multiplication process in which from each isolated ripple seed, secondary satellite ripples are created by downward excavation of the wetting

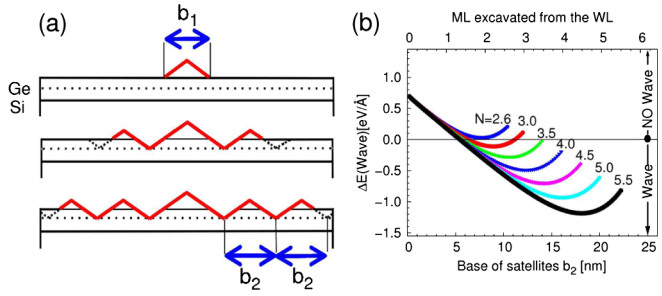

FIG. 4 (color online). (a) Wave propagation mechanism starting from an isolated ripple (top) on a WL, creating first two asymmetric satellites (middle) with satellite base b_2, finally leading to full faceting (bottom). (b) Energy difference between the configurations of the single ripple with $b_1 = 10$ nm and the ripple with two satellite ripples as a function of the final satellite base b_2 for different N values.

layer at the ripple edges. The resulting lateral motion of material rapidly transforms the film to a completely faceted WL. In Fig. 4(b), the total energy difference between the initial single ripple configuration with $b_1 = 10$ nm and the ripple with two adjacent satellite ripples is plotted for different values of N as a function of increasing satellite base b_2 as the trenches are downward excavated. For a transformed material of $N = 4.5$ ML [upper scale of Fig. 4(b)], we see that the system smoothly evolves to satellite ripples with preferred base $b_2 \approx 15$ nm, leaving a residual WL thickness less than 1 ML underneath. The process repeats for all further satellite ripples and thus, triggers a rapid surface transformation in which nearly all deposited material is absorbed in the ripple structure and the original (1110) surface is erased. The predicted favored ripple width b as well as the residual WL thickness underneath nicely agree with the experimental values. Moreover, the energetically favored ripple width b_2 turns out to be practically independent of the initial seed ripple width b_1, which is an important factor that promotes a high uniformity of the final ripple structure.

In conclusion, our experimental and theoretical results imply that the faceted film corresponds to a new type of wetting layer rather than a SK configuration. Therefore, the usual monotone evolution of SK seeds to 3D islands during the initial deposition stages is strongly altered on the vicinal (1110) surface. Such an anomaly should be present also in other systems whenever peculiar shallow facets displaying geometric degeneracy and low surface energy densities compared to the substrate are present. At higher coverages and temperatures, eventually a transition to dome islands with steeper side facets will occur, as then energetics are dominated by elastic effects. Our work has also revealed an effective pathway for the abrupt faceting process and we have originally provided a first experimentally derived estimate for the edge energy of {105} facets with nonsharp junctions, serving as a reference for other edge energies in SK systems that are presently far off to be computed by *ab initio* approaches.

This work was supported by the Austrian Science Funds (SFB-IRON) and the Gesellschaft für Mikro- und Nanoelektronik, Vienna.

*Corresponding author.
gunther.springholz@jku.at

[1] J. Tersoff and F. K. LeGoues, Phys. Rev. Lett. **72**, 3570 (1994).
[2] I. Daruka, J. Tersoff, and A.-L. Barabási, Phys. Rev. Lett. **82**, 2753 (1999).
[3] G. Medeiros-Ribeiro *et al.*, Science **279**, 353 (1998).
[4] F. Ross, R. M. Tromp, and M. C. Reuter, Science **286**, 1931 (1999).
[5] E. Sutter, P. Sutter, and J. E. Bernard, Appl. Phys. Lett. **84**, 2262 (2004).
[6] G. Costantini *et al.*, Appl. Phys. Lett. **85**, 5673 (2004).
[7] J. T. Robinson *et al.*, Nanotechnology **20**, 085708 (2009).
[8] O. E. Shklyaev *et al.*, Phys. Rev. Lett. **94**, 176102 (2005).
[9] M. Brehm *et al.*, Phys. Rev. B **80**, 205321 (2009).
[10] Y. W. Mo *et al.*, Phys. Rev. Lett. **65**, 1020 (1990).
[11] M. Brehm *et al.*, Nano. Res. Lett. **6**, 70 (2011).
[12] C. Teichert, J. C. Bean, and M. G. Lagally, Appl. Phys. A **67**, 675 (1998).
[13] P. Sutter, E. Sutter, and L. Vescan, Appl. Phys. Lett. **87**, 161916 (2005).
[14] F. Watanabe *et al.*, Appl. Phys. Lett. **85**, 1238 (2004).
[15] P. D. Szkutnik *et al.*, Phys. Rev. B **75**, 033305 (2007).
[16] B. Sanduijav *et al.*, Phys. Rev. B **80**, 125329 (2009).
[17] L. Persichetti *et al.*, Phys. Rev. Lett. **104**, 036104 (2010).
[18] G. Chen *et al.*, Appl. Phys. Lett. **96**, 103107 (2010).
[19] C. M. Retford *et al.*, Phys. Rev. B **75**, 075311 (2007).
[20] E. Levy *et al.*, Phys. Rev. Lett. **97**, 196802 (2006).
[21] See, e.g., R. Rurali, Rev. Mod. Phys. **82**, 427 (2010), and references therein.
[22] G. Capellini, M. De Seta, and F. Evangelisti, Appl. Phys. Lett. **78**, 303 (2001).
[23] O. G. Schmidt *et al.*, Appl. Phys. Lett. **81**, 2614 (2002); U. Denker, H. Sigg, and O. G. Schmidt, Appl. Surf. Sci. **224**, 127 (2004).
[24] A. A. Baski, S. C. Erwin, and L. J. Whitman, Surf. Sci. **392**, 69 (1997).
[25] D. J. Chadi, Phys. Rev. Lett. **59**, 1691 (1987).
[26] A. Rastelli *et al.*, Phys. Rev. B **68**, 115301 (2003).
[27] Y. Fujikawa *et al.*, Phys. Rev. Lett. **88**, 176101 (2002).
[28] P. Raiteri *et al.*, Phys. Rev. Lett. **88**, 256103 (2002).
[29] D. B. Migas *et al.*, Surf. Sci. **556**, 121 (2004).
[30] D. Scopece, F. Montalenti, and M. J. Beck (to be published).
[31] Annealing results will be reported elsewhere.